Theoretical Mn K-edge XANES for Li_2MnO_3: DFT+U study

Tomoyuki Tamura[1], Tsukuru Ohwaki[2], Atsushi Ito[2], Yasuhiko Ohsawa[2], Ryo Kobayashi[3], and Shuji Ogata[3]

[1] Center for Fostering Young and Innovative Researchers, Nagoya Institute of Technology, Gokiso, Showa, Nagoya, Aichi 466-8555, Japan
[2] Nissan Research Center, Nissan Motor Co., Ltd., 1, Natsushima-cho, Yokosuka, Kanagawa 237-8523, Japan
[3] Graduate School of Engineering, Nagoya Institute of Technology, Gokiso, Showa, Nagoya, Aichi 466-8555, Japan

E-mail: tamura.tomoyuki@nitech.ac.jp

Abstract. Spectral features of Mn K-edge X-ray absorption near-edge structure (XANES) for Li_2MnO_3 were calculated using first-principles full-PAW method with general gradient approximation (GGA) plus U method. We demonstrated that the U parameter affects the spectral features in the pre-edge region while that does not affect those in the major absorption region. From the comparison with the experimental spectra and those of reference compounds, we showed that the spectral features of Mn K-edge XANES and the differences in the valence state can be well reproduced.

1. Introduction

High performance Li-ion batteries have been indispensable as one of key components of a new electric motorization due to its high energy efficiency. To increase the specific energy of Li-ion batteries, it is necessary to increase the capacity of the cathode. It has been reported that the Li-rich solid-solution layered cathode material Li_2MnO_3-LiMO$_2$ (M=Co, Ni etc.) exhibits a discharge capacity greater than 200mA·h/g when operated above 4.6 V, making it a promising candidate for the cathode material [1]. In addition, atomic-resolution scanning transmission electron microscopy (STEM) observations revealed that some of the transition metal (TM) atoms were transferred from the TM layers to the Li layers during the first charge and discharge, leading to the partial formation of a framework structure, probably a spinel structure, and the formation of this framework structure should be closely related to the cyclic durability [2]. However, the detailed mechanism is still unclear. For the further increase of the performance of Li-ion batteries, the mechanism of the charge-discharge reaction in the cathode material should be clarified. We have analyzed the changes in valence state of Ni, Co, and Mn in $Li[Ni_{0.17}Li_{0.2}Co_{0.07}Mn_{0.56}]O_2$ during the charge-discharge process in detail using in situ X-ray absorption spectroscopy (XAS), which includes both X-ray absorption near-edge structure (XANES) and extended X-ray absorption fine structure (EXAFS) measurements [3]. The shifts in the Ni K-edge XANES are approximately parallel during the charge-discharge process, and the valence state of Ni should change between 2+ and almost 4+. On the other hand, the shape of the Mn K-edge XANES appears to be characteristic compared to that of Ni, where one part of

the Mn K-edge main absorption near the inflection point moves in the opposite direction of the other parts during the charge-discharge process. It thus appears to be somewhat complicated to discuss the valence change of Mn from only the experimental spectra. The basic change in the global pattern for Co is similar to that of Mn. Although it may be possible to clarify the charge-discharge reaction mechanism via the detailed interpretation of experimental results, it has not been achieved.

Reliable theoretical spectra might be useful to interpret the complicated spectral changes observed experimentally. A lot of attempts have been performed to develop reliable theoretical scheme to reproduce XANES spectra. There are two kinds of approaches that can deal with realistic defective models, such as defects. One is multiple scattering approach [4, 5], which basically deals with scattering phenomena of an excited electron associated with the X-ray absorption. This approach works in the real space description and is a standard technique for analyzing both XANES and EXAFS (extended X-ray absorption fine structure) within the same theoretical framework by varying the energy of the excited electron. The other approach is the band-structure methods, where the transition matrix between initial (ground) and final (excited) states is dealt with within the framework of the density functional theory (DFT) [6, 7]. Computations are performed in the reciprocal space description under the periodic boundary condition. The band-structure methods have an advantage that various physical quantities can be derived in the same theoretical framework, such as total energies, stable atomic configurations, electron densities, band structure diagrams, and densities of states. This allows combined interpretation of these physical properties with the XANES spectra. This kind of approach has been applied with the orthogonalized linear combination of atomic orbital (OLCAO) method [8, 9], the full-potential linearized augmented plane-wave (FLAPW)+local orbitals (lo) method [10], and the pseudopotential method [11, 12, 13, 14]. In the band-structure methods, the interactions between a core hole and electrons are dealt with through the inclusion of an excited atom into a supercell [8, 9]. It is desirable to deal with enough large supercells, so as to prevent unphysical strong interactions among the excited atoms in repeated cells. This point as well as the need of realistic structural models requires huge computational efforts. Thus the scheme to utilize the pseudopotential method is superior so as to reduce the computational efforts for large supercells. However, in such a scheme, the reconstruction of true all-electron (AE) valence wave functions from pseudo-wave functions based on the concept of projector augmented-wave (PAW) approach [15, 16, 17] is essential to obtain the transition matrix elements accurately [11, 12, 13, 14]. Thus we have developed a XANES simulation code by the full usage of the PAW method, such as the computations of the electronic structures of excited and ground-state supercells, the transition matrix, and the threshold energy, and have installed it into our PAW code, QMAS (Quantum MAterials Simulator) [18].

It is well known that DFT within the standard local-density approximation (LDA) or generalized gradient approximation (GGA) to the exchange and correlation functional, experiences severe limitations in describing the physics of magnetic materials with strongly localized electron states. Many different methods have been proposed to overcome this fundamental limitation of standard DFT approaches, varying from the rather popular DFT+U method [19] to the more sophisticated self-interaction corrections (SIC) [20] and Green's-function-based (GW) approaches [21]. Recently, the hybrid Hartree-Fock DFT approaches [22] have been proposed. For relatively large supercells for a defective model including Li removal, the DFT+U method is the most practical in terms of the computational efforts. The use of this method in calculating physical properties such as redox potentials for Li-insertion [23] suffers from the unavoidable compromise in the choice of U values, and the scheme to calculate U values self-consistently has been proposed.

In this paper, we demonstrate the theoretical Mn K-edge XANES spectra for Li_2MnO_3, and compare them with other reference compounds. We study the effects of the Hubbard parameter

U on the spectral features of Mn K-edge. To our knowledge, there is no theoretical study of Mn K-edge spectra for this compound.

2. Computational details

The present calculations are performed by using our computational code QMAS [18]. We adopted the PAW method with GGA for the exchange-correlation interactions and GGA+U [19] with the effective Hubbard-U parameter $U_{\rm eff} = U - J$, simply U afterwards, for Mn $3d$ orbitals. We varied the U values around 5.0 eV, between 3.0 and 7.0 eV, since the electronic structures of delithiated Li_2MnO_3 have been discussed with U=5.0 eV [24], which was theoretically estimated for Mn^{4+} in spinel-type MnO_2 [23]. The plane-wave energy cutoff was set to 544.2 eV (20.0 hartree). The calculations of the orbital-decomposed partial density of states (PDOS) were performed using a projection of the plane-wave states onto a localized linear combination of atomic-orbitals basis set [25].

The structure identification of Li_2MnO_3 has been reported using the space-group symmetry of $C2/m$ [26], where Wyckoff positions are $2b$, $2c$, and $4h$ for the Li ions, $4g$ for the Mn ion, and $4i$ and $8j$ for the O ions. For the self-consistent calculations, the number of $\mathbf{k}$ points was set to 6×4×6 in the Brillouin zone. We considered the antiferromagnetic arrangement, in which the Mn atoms in one Mn-rich layer are aligned anti-parallel.

The proper inclusion of a core hole in the supercell is essential to reproduce the experimental transition-metal K-edge spectra such as Co K-edge XANES for $LiCoO_2$ [27]. The core-hole effect can be dealt with through the PAW pseudopotential of an excited atom with a core hole. The PAW pseudopotential, namely, the set of a local potential, projectors, and pseudo- and AE-partial waves of the target atom is constructed for a free atom with a core $1s$ electron excited into a lowest unoccupied orbital, which results in the increase in the valence number of the PAW pseudopotential. To obtain the excited-state wave functions, we perform self-consistent calculations of the supercell containing an excited atom, where the atomic configuration is fixed as that in the ground state due to the rapid excitation process. In the supercell, one extra valence electron is added to the lowest unoccupied state so as to compensate the increase in the valence number at the excited atom [8, 9].

The intensity distribution of K-edge XANES within the dipole approximation can be approximately obtained by

$$\mu \propto \sum_{\mathbf{k},n\in \mathrm{cb}} \left|\langle \psi^n_{\mathbf{k}} | \mathbf{e}\cdot\mathbf{r} | \psi^{1s}\rangle\right|^2 \delta(E - E^n_{\mathbf{k}} + E^{1s}), \tag{1}$$

where $\mathbf{e}$ is the unit vector for the polarization direction of the X-ray, and $\psi^n_{\mathbf{k}}$ is the excited-state wavefunction of the conduction band n at $\mathbf{k}$ in the Brillouin zone of the supercell [28, 29]. In the PAW method, the AE wave function $\psi^n_{\mathbf{k}}$ obtained from the self-consistent calculation of the supercell can be directly used in the transition matrix. The K-edge spectrum is given by the excitation from a core $1s$ state. ψ^{1s} in the transition matrix is the $1s$ atomic orbital of the target atom in the supercell. E^{1s} and $E^n_{\mathbf{k}}$ denote Kohn-Sham energies of the ground and excited states, respectively. Practically, E^{1s} is not used, because the threshold energy $E_{\rm th}$ obtained separately is used as the difference between E^{1s} and the lowest $E^n_{\mathbf{k}}$ ($E^{\rm CBM}$) as:

$$E^n_{\mathbf{k}} - E^{1s} = E^n_{\mathbf{k}} - E^{\rm CBM} + E_{\rm th}, \tag{2}$$

where $E_{\rm th}$ is given as the total energy difference between the excited and ground state, which are obtained by a separate set of calculations as follows:

$$E_{\rm th} \approx \Delta E^{\rm valence}_{\rm cell} + \Delta E^{\rm core}_{\rm atom} \tag{3}$$

$$\Delta E^{\rm valence}_{\rm cell} = E^{\rm valence}_{\rm cell}[\text{core hole},\ N+1] - E^{\rm valence}_{\rm cell}[N] \tag{4}$$

$$\Delta E^{\rm core}_{\rm atom} = E^{\rm core}_{\rm atom}[\text{core hole},\ n-1] - E^{\rm core}_{\rm atom}[n]. \tag{5}$$

Eq. (4) represents the total energy difference between the excited and ground-state supercells in the PAW scheme. The excited atom is represented by the excited PAW pseudopotential with an increased valence number, which is neutralized by an extra valence electron as $N+1$ in the supercell. The total energies $E_{\rm cell}^{\rm valence}$ are calculated for valence electrons and ions, and $\Delta E_{\rm cell}^{\rm valence}$ does not directly contain the energy changes of core electrons. This is complemented by $\Delta E_{\rm atom}^{\rm core}$ given in Eq. (5) as the total-energy difference of core electrons between the core-hole system with $n-1$ core electrons and the ground state with n core electrons at the target atom. $\Delta E_{\rm atom}^{\rm core}$ is obtained by the isolated atom calculation, which is performed when generating the PAW pseudopotential. We have confirmed that the calculated chemical shifts in Ti and O K-edge for Ti-bearing crystalline oxides and Ti-doped SiO_2 glasses using these formulations show satisfactory agreement with experimental results [30].

We use a supercell of 2×1×2 unitcells so as to prevent unphysical strong interactions among the excited atoms with a core hole in repeated cells. The number of **k** points was set to 4×3×4. The theoretical spectra are broadened with Gaussian functions of the full width at half maximum of 0.5 eV to separate clearly the peaks in Fig. 3 and 0.8 eV to compare with the experimental spectra in Fig. 4.

3. Results and discussion

Table 1. Structure parameters for Li_2MnO_3.

U (eV)	a (Å)	b (Å)	c (Å)	$\beta(^\circ)$
GGA	4.957	8.567	5.046	109.45
3.0	4.967	8.584	5.054	109.47
4.0	4.971	8.591	5.056	109.48
5.0	4.976	8.600	5.060	109.49
6.0	4.977	8.601	5.066	109.49
7.0	4.990	8.622	5.069	109.50
Calc. [24]	5.020	8.676	5.093	109.50
Exp. [26]	4.937	8.532	5.030	109.46

The calculated structure parameters for Li_2MnO_3 are summarized in Table 1. With the increase of U values, the lattice constants and the lattice angles increase slightly. The latice constants are overestimated by 1% compared with the experimental results. This is a reasonable error for the use of GGA+U.

Figure 1 shows the total density of states (TDOS) and PDOS in Li_2MnO_3 for U=5.0 eV. The valence band mainly consists of Mn 3d and O 2p states, and the conduction band mainly consists of Mn 3d, Mn 4sp, and Li 2sp states. Mn 3d states are split into the two group, d_{xy}, d_{yz}, and d_{zx} denoted as t_{2g} states in a perfect octahedron, and $d_{x^2-y^2}$ and $d_{z^2-r^2}$ denoted as e_g states. The e_g orbitals point toward oxygen atoms, while the t_{2g} orbitals point toward the midpoints of oxygen atoms. In the valence band, the interaction between the Mn majority-spin t_{2g} states and O 2p states generate the weak π bonding states at the bottom around -5 eV, the interaction between the Mn majority-spin e_g states and O 2p states generates the σ bonding states in the middle around -4 eV, and the O nonbonding 2p states are located at the top region. In the conduction band, the Mn majority-spin e_g states and the Mn minority-spin t_{2g} and e_g states are formed at the lower part ($3 \sim 5$ eV), and the dispersed Li 2sp band hybridized with Mn 4sp orbitals are formed at the higher part above 9 eV. The band gap results from the energy

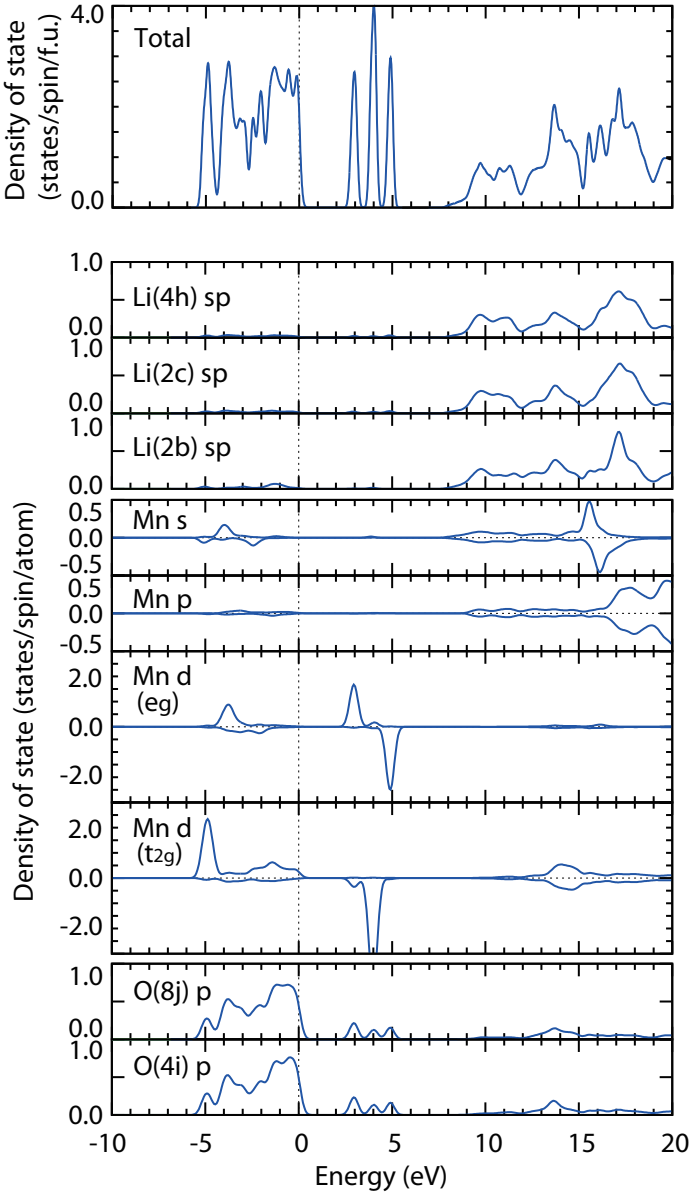

Figure 1. Total density of states and orbital-decomposed partial density of states for Li_2MnO_3 for $U = 5.0$ eV in the local coordinate system. The top of the valence band is chosen as 0 eV.

difference between the occupied O nonbonding $2p$ states and the unoccupied Mn majority-spin e_g states

Figure 2 shows the dependence of total DOS on U values. With the increase of U values, the occupied Mn majority-spin t_{2g} state shifts to lower energy and the unoccupied Mn minority-spin t_{2g} state shifts to higher energy. Shifts of Mn e_g states are smaller than those of Mn t_{2g}, which results in a small change of the band gap. This is quite different from $LiCoO_2$ in a similar layered lock-salt structure, where the band gap comes from the energy difference between Co occupied t_{2g} and unoccupied e_g states [27]. Mn t_{2g} electrons are not so delocalized since Mn t_{2g}-O $2p$ hybridization is weak, while the e_g electrons are more delocalized than t_{2g} states due to the hybridization with O $2p$. These result in the smaller effects of U values on Mn e_g states.

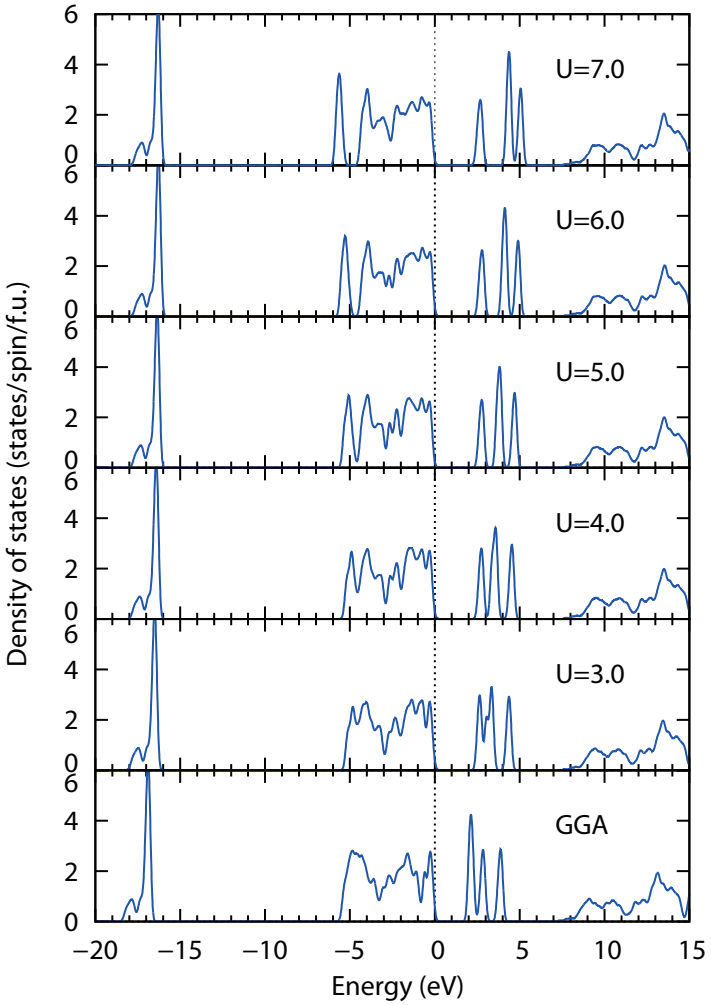

Figure 2. Total density of states for Li_2MnO_3 as a function of U values. The top of the valence band is chosen as 0 eV.

For example, a separate treatment of t_{2g} and e_g electrons on transition-metal sites as localized and itinerant, respectively, give an appropriate description for the band structure of LaMO$_3$ perovskites (M=Ti-Cu) [31].

Figure 3 shows theoretical Mn K-edge spectra for U=3.0, 5.0 and 7.0 eV, and the calculated threshold energies for these spectra are listed in Table 2. With the increase of U values, the threshold energies decrease slightly. The spectral shape of Mn K-edge is similar to that of unoccupied Mn p PDOSs shown in Fig. 1. Spectra can be separated into two parts, i.e., the pre-edge part and the major absorption part. The pre-edge region is focused on in the inbox. It is well-known that the pre-edge features of transition-metal (TM) K-edge are very sensitive to the geometry of TM-centered polyhedra, and those are widely used to determine coordination numbers despite weak intensities [32]. The highest pre-edge peak shifts to a higher energy with the increase of the U value, and the pre-edge peaks split into two parts for U=7.0 eV. This should come from the shift of unoccupied Mn minority-spin t_{2g} state shown in Fig. 2. Mn K-edge should mainly come from the Mn $1s \rightarrow 4p$ transition within the dipole approximation. However, lower conduction bands are mainly formed by Mn $3d$ orbitals as shown in Fig. 1. The weak pre-edge peaks can be interpreted in terms of the hybridization between Mn $4p$ and

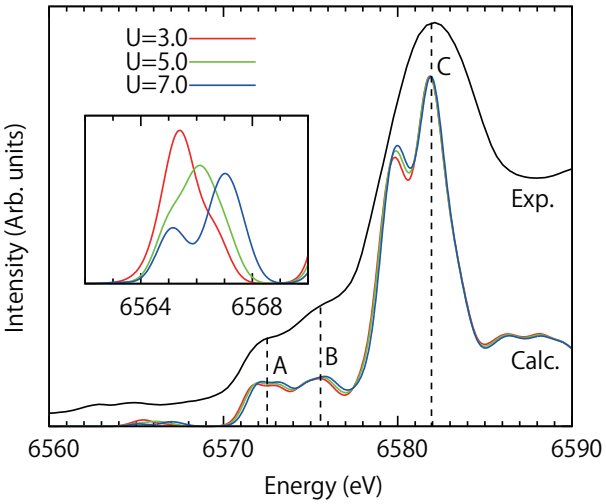

Figure 3. Theoretical Mn K-edge spectra for U=3.0, 5.0 and 7.0 eV in comparison with the experimental spectrum [3] which is shifted to match the peak C.

Mn 3d orbitals due to the octahedral symmetry. In the major absorption part, slight changes in the intensity can be seen around 6580 eV. When theoretical spectra are compared with the experimental one, these changes are negligible. Since higher conduction bands are mainly formed by unoccupied Mn 4sp and Li 2sp orbitals, these bands are not affected significantly by the U values.

Table 2. Calculated threshold energies $E_{\rm th}$ of Mn K-edge for Li_2MnO_3.

U (eV)	$E_{\rm th}$ (eV)
3.0	6563.53
5.0	6563.39
7.0	6563.22

To study the effects of changes in Mn valence-state, we compare the theoretical Mn K-edge spectra with reference compounds, bulk MnO and β-MnO_2, and with experimental spectra in Fig. 4. The U parameter used was 5.0 eV for all compounds. The formal Mn valence-states in MnO, MnO_2, and Li_2MnO_3 are +2, +4, and +4, respectively. As experimentally observed, the theoretical spectrum for a smaller Mn valence-state is located at a lower energy side. This means that the changes in Mn valence-state can be well reproduced. Furthermore, the theoretical spectra of Li_2MnO_3 and MnO_2 in the same Mn valence-state are crossing in the lower part of the major absorption around 6574 eV, as observed in the experimental spectra. This means that the effects of the local structural changes can be well reproduced, and we obtained the reliable theoretical spectra for studying the spectral changes experimentally observed. In the present calculations, the quadrupolar transitions are not taken into account. These effects can be seen in the pre-edge region as shown in the inboxes of Fig. 4, where two peaks exist in the experimental spectra while only one peak exists in the theoretical ones. The effects of the inclusion of the quadrupolar transitions have been discussed for the Ti K-edge XANES spectra, and it has been

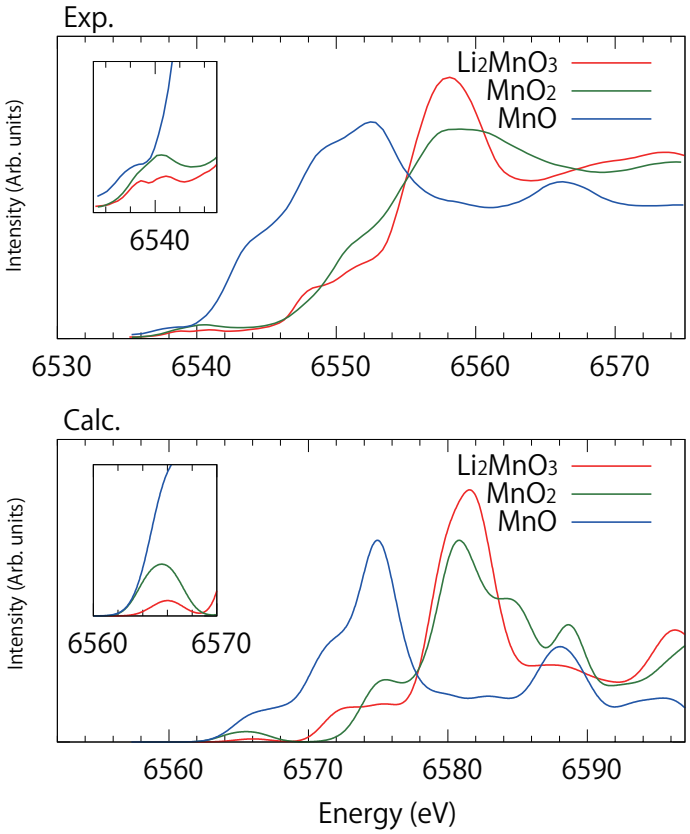

Figure 4. Theoretical Mn K-edge for MnO, MnO_2, and Li_2MnO_3 for U=5.0 eV in comparison with experimental spectra [3].

concluded the quadrupole $1s \rightarrow 3d$ transition generates a weak peak below the lowest peak by the dipole transition [33, 34]. Since the split of the pre-edge peak for U=7.0 eV shown in Fig. 3 disappears with larger broadening parameter, this split does not correspond to the experimental one shown in Fig. 4. The spectral features of pre-edge peaks in Mn K-edge should be discussed with the inclusion of the quadrupolar transitions. However, note that spectral features other than peaks originated from the quadrupolar transitions can be well reproduced within the present dipole approximation.

4. Conclusions

We performed first-principles full-PAW calculations of Mn K-edge XANES spectra for Li_2MnO_3 with GGA+U method. We demonstrated that the U parameter affects the spectral features in the pre-edge region while that does not affect those in the major absorption region. From the comparison with the experimental spectra and those of reference compounds, we show that the spectral features of Mn K-edge XANES and the differences in the valence state can be well reproduced. We are working on the effects of Li removals and phase transitions on the spectral features, and the charge-discharge reaction mechanism will thereby be clarified via the combined interpretation of experimental and theoretical results.

Acknowledgments
We would like to thank S. Tanaka and M. Kohyama for their helpful discussions. The application part of this work was supported by New Energy and Industrial Technology Development Organization (NEDO) and the developing a computational code was supported by the Strategic Programs for Innovative Research (SPIRE).

References

[1] Ito A, Li D, Sato Y, Arao M, Watanabe M, Hatano M, Horie H and Ohsawa Y 2010 *J. Power Sources* **195** 567
[2] Ito A, Shoda K, Sato Y, Hatano M, Horie H and Ohsawa Y 2011 *J. Power Sources* **196** 4785
[3] Ito A, Sato Y, Sanada T, Hatano M, Horie H and Ohsawa Y 2011 *J. Power Sources* **196** 6828
[4] Rehr J J, Kas J J, Prange M P, Sorini A, Takimoto Y and Vila F 2009 *Compte Rendus Physique* **10** 548
[5] Filipponi A, Cocco A D and Natoli C R 1995 *Rhys. Rev. B* **52** 15122
[6] Hohenberg P and Kohn W 1964 *Phys. Rev.* **136** B864
[7] Kohn W and Sham L J 1965 *Phys. Rev.* **140** A1133
[8] Mo S D and Ching W Y 2000 *Phys. Rev. B* **62** 7901
[9] Mo S D and Ching W Y 2001 *Appl. Phys. Lett.* **78** 3809
[10] Hébert C 2007 *Micron* **38** 12 and references therein
[11] Pickard C J 1997 PhD thesis University of Cambridge
[12] Jayawardane D, Pickard C, Brown L and Payne M 2001 *Phys. Rev. B* **64** 115107
[13] Suenaga K, Sandré E, Colliex C, Pickard C J, Kataura H and Iijima S 2001 *Phys. Rev. B* **63** 165408
[14] Taillefumier M, Cabaret D, Flank A M and Mauri F 2002 *Phys. Rev. B* **66** 195107
[15] Blöchl P E 1994 *Phys. Rev. B* **50** 17953
[16] Holzwarth N, Matthews G, Dunning R, Tackett A and Zeng Y 1997 *Phys. Rev. B* **55** 2005
[17] Kresse G and Joubert D 1999 *Phys. Rev. B* **59** 1758
[18] http://www.qmas.jp
[19] Anisimov V I, Zaanen J and Anderson O K 1991 *Phys. Rev. B* **44** 943
[20] Svane A and Gunnarsson O 1990 *Phys. Rev. Lett.* **65** 1148
[21] Hedin L 1965 *Phys. Rev.* **139** A796
[22] Becke A D 1993 *J. Chem. Phys.* **98** 1372
[23] Zhou F, Cococcioni M, Marianetti C A, Morgan D and Ceder G 2004 *Phys. Rev. B* **70** 235121
[24] Koyama Y, Tanaka I, Nagao M and Kanno R 2009 *J. Power Sources* **189** 798
[25] Sanchez-Portal D, Artacho E and Soler J M 1995 *Solid State Commun.* **95** 685
[26] Strobel P and Lambert-Andron B 1988 *J. Solid State Chem* **75** 90
[27] Juhin A, Groot F and Vankó G 2010 *Phys. Rev. B* **81** 115115
[28] Tanaka I, Mizoguchi T and Yamamoto T 2005 *J. Am. Ceram. Soc.* **88** 2013
[29] Mizoguchi T, Olovsson W, Ikeno H and Tanaka I 2010 *Micron* **41** 695
[30] Tamura T, Tanaka S and Kohyama M 2011 *Phys. Rev. B* submitted
[31] Solovyev I, Hamada N and Terakura K 1996 *Phys. Rev. B* **53** 7158
[32] Farges F 2005 *Phys. Rev. B* **71** 155109
[33] Joly Y, Cabaret D, Renevier H and Natoli C R 1999 *Phys. Rev. Lett.* **82** 2398
[34] Yamamoto T, Mizoguchi T and Tanaka I 2005 *Phys. Rev. B* **71** 245113